1521-0111/96/4/485–492$35.00
MOLECULAR PHARMACOLOGY

https://doi.org/10.1124/mol.119.117531
Mol Pharmacol 96:485–492, October 2019

ACCELERATED COMMUNICATION

Structural Basis for Diltiazem Block of a Voltage-Gated Ca^{2+} Channel[S]

Lin Tang, Tamer M. Gamal El-Din, Michael J. Lenaeus, Ning Zheng,[1] and William A. Catterall[1]

Department of Neurology, State Key Laboratory of Biotherapy and Cancer Center, West China Hospital, Sichuan University and Collaborative Innovation Center for Biotherapy, Chengdu, Sichuan, China (L.T.); and Department of Pharmacology (L.T., T.M.G.E.-D., M.J.L., N.Z., W.A.C.), Division of General Internal Medicine, Department of Medicine (M.J.L.), and Howard Hughes Medical Institute (N.Z.), University of Washington, Seattle, Washington

Received June 13, 2019; accepted August 2, 2019

ABSTRACT

Diltiazem is a widely prescribed Ca^{2+} antagonist drug for cardiac arrhythmia, hypertension, and angina pectoris. Using the ancestral Ca_V channel construct Ca_VAb as a molecular model for X-ray crystallographic analysis, we show here that diltiazem targets the central cavity of the voltage-gated Ca^{2+} channel underneath its selectivity filter and physically blocks ion conduction. The diltiazem-binding site overlaps with the receptor site for phenylalkylamine Ca^{2+} antagonist drugs such as verapamil. The dihydropyridine Ca^{2+} channel blocker amlodipine binds at a distinct site and allosterically modulates the binding sites for diltiazem and Ca^{2+}. Our studies resolve two distinct binding poses for diltiazem in the absence and presence of amlodipine. The binding pose in the presence of amlodipine may mimic a high-affinity binding configuration induced by voltage-dependent inactivation, which is favored by dihydropyridine binding. In this binding pose, the tertiary amino group of diltiazem projects upward into the inner end of the ion selectivity filter, interacts with ion coordination Site 3 formed by the backbone carbonyls of T175, and alters binding of Ca^{2+} to ion coordination Sites 1 and 2. Altogether, our results define the receptor site for diltiazem and elucidate the mechanisms for pore block and allosteric modulation by other Ca^{2+} channel–blocking drugs at the atomic level.

SIGNIFICANCE STATEMENT

Calcium antagonist drugs that block voltage-gated calcium channels in heart and vascular smooth muscle are widely used in the treatment of cardiovascular diseases. Our results reveal the chemical details of diltiazem binding in a blocking position in the pore of a model calcium channel and show that binding of another calcium antagonist drug alters binding of diltiazem and calcium. This structural information defines the mechanism of drug action at the atomic level and provides a molecular template for future drug discovery.

Introduction

Benzothiazepines (BZTs), 1,4-dihydropyridines (DHPs), and phenylalkylamines (PAAs) are three major classes of voltage-gated Ca^{2+} channel blockers, which are widely used in the therapy of cardiovascular disorders, such as hypertension, angina pectoris, and cardiac arrhythmia (Triggle, 2007; Zamponi et al., 2015; Godfraind, 2017). These therapeutic agents were first introduced into clinical practice 40 years ago and are still prescribed to millions of patients. Diltiazem belongs to the BZT class of Ca^{2+} channel antagonists and has been shown to inhibit the L-type Ca^{2+} currents conducted by $Ca_V1.2$ channels in cardiac and vascular smooth muscle in a voltage- and activity-dependent manner (Lee and Tsien, 1983; Hondeghem and Katzung, 1984; Hockerman et al., 1997; Catterall, 2000; Zamponi et al., 2015), similar to local anesthetics acting on Na_V channels (Hille, 1977). The mechanisms of action of representative DHPs and PAAs at two distinct receptor sites on Ca^{2+} channels have been elucidated at the structural level (Tang et al., 2016). Diltiazem is receiving increased clinical use (Tamariz and Bass, 2004), but how it targets the Ca^{2+} channel, induces state-dependent block, and interacts allosterically with bound Ca^{2+}, DHPs, and PAAs remains elusive.

The research reported in this publication was supported by the National Institutes of Health National Heart, Lung, and Blood Institute [Award R01HL112808] (to W.A.C. and N.Z.) and National Institute of Neurologic Disorders and Stroke [Award R01NS015751] (to W.A.C.). The content is solely the responsibility of the authors and does not necessarily represent the official views of the National Institutes of Health. This work was also supported by the Howard Hughes Medical Institute (to N.Z.).
The authors declare no competing financial interests.
[1]W.A.C. and N.Z. are co-senior authors.
https://doi.org/10.1124/mol.119.117531.
[S] This article has supplemental material available at molpharm.aspetjournals.org.

ABBREVIATIONS: BZT, benzothiazepine; DHP, dihydropyridine; PAA, phenylalkylamine.

Mammalian voltage-gated Ca^{2+} channels consist of four homologous six-transmembrane domains that form a central pore with four surrounding voltage-sensor modules (Catterall, 2011; Zamponi et al., 2015). These channels most likely evolved from a prokaryotic ancestor, which is exemplified by the homotetrameric bacterial voltage-gated sodium channel, Na_VAb (Ren et al., 2001; Payandeh et al., 2011, 2012). By re-engineering the selectivity filter of Na_VAb, we constructed a model Ca^{2+}-selective channel, Ca_VAb, to decipher the structural basis of ion selectivity and conductance and the mechanism of inhibition by DHPs and PAAs (Tang et al., 2014, 2016). We found that Ca_VAb mimics the Ca^{2+} selectivity of mammalian cardiac $Ca_V1.2$ channels exactly, which allowed us to image bound Ca^{2+} in the pore and define the conductance mechanism (Tang et al., 2014). We also found that Ca_VAb is blocked by PAAs and DHPs with similar mechanisms and affinities as mammalian $Ca_V1.2$ channels, and we defined the separate binding sites for these two distinct classes of Ca^{2+} antagonist drugs and elucidated their allosteric interactions (Tang et al., 2016). In our previous work, we were unable to solve the crystal structure of Ca_VAb with diltiazem bound at high resolution. Here, using improved biochemical and crystallographic methods, we reveal the structural basis for diltiazem block of Ca_VAb channels by X-ray crystallography and define the molecular mechanism for allosteric coupling among the binding sites for Ca^{2+}, DHPs, and BZTs.

Materials and Methods

In brief summary, Ca_VAb and its derivative constructs were expressed in *Trichopulsia ni* insect cells and purified using anti-Flag resin and size exclusion chromatography, reconstituted into 1,2-dimyristoyl-sn-glycero-3-phosphocholine and 3-[(3-cholamidopropyl) dimethylammonio]-2-hydroxy-1-propanesulfonate bicelles, and crystallized over an ammonium sulfate solution containing 0.1 M Na-citrate (pH 5.0) in the presence of drugs of interest. The tertiary complex of diltiazem-CavAb-DHP was prepared by addition of diltiazem from the beginning of purification, and addition of the second drug (DHP) before reconstitution into the 1,2-dimyristoyl-sn-glycero-3-phosphocholine and 3-[(3-cholamidopropyl)dimethylammonio]-2-hydroxy-1-propanesulfonate bicelles. The data sets for the diltiazem-bound complex and the tertiary complexes of diltiazem-Ca_VAb-DHP were collected at 1.0 Å wavelength at advanced light source. Electrophysiological experiments were performed in *Trichopulsia ni* cells using standard protocols. Details of our methods are provided online in the Supplemental Material. Coordinates and structure factors have been deposited in the Protein Data Bank under accession codes 6KE5 and 6KEB.

Results

State-Dependent Inhibition of Ca_VAb by Diltiazem. The structure of diltiazem (Fig. 1A) and related benzothiazepines differs substantially from PAAs and DHPs. Nevertheless, ligand-binding and site-directed mutagenesis studies suggest that the receptor sites for PAAs and BZTs overlap at least partially (Kraus et al., 1996; Hockerman et al., 2000; Dilmac et al., 2003). Similar to other Ca^{2+}-channel blockers, diltiazem inhibits Ca_VAb in a complex state-dependent way. It blocks the channel in its resting state with an IC_{50} value of 41 μM (Fig. 1, B and D, green). In contrast, its inhibitory effect is strengthened by repetitive depolarizing stimuli that activate and inactivate the channel, yielding an increased potency of 10.4 μM for use-dependent block (Fig. 1, B and D, black).

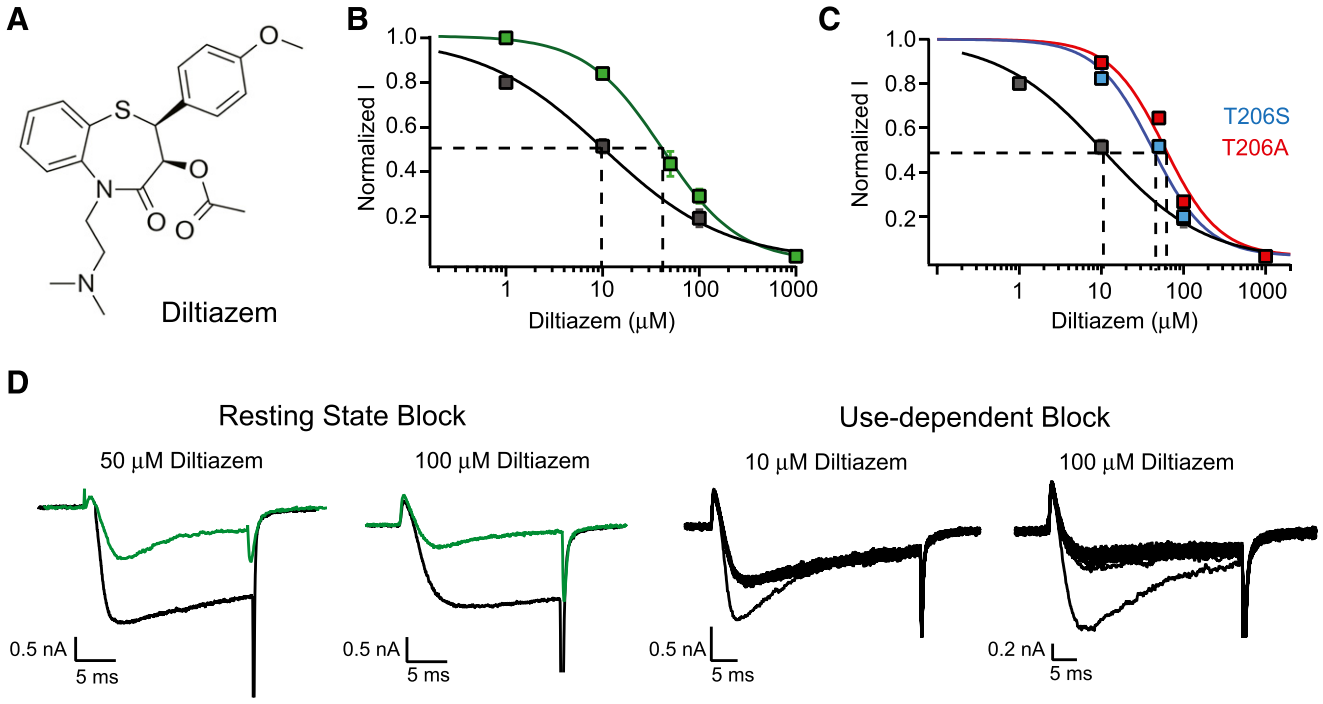

Fig. 1. Ca_VAb block by diltiazem. (A) Structural formula of diltiazem. (B) Concentration curves for inhibition of Ca_VAb by diltiazem in the resting state (green) at a holding potential of −120 mV with IC_{50} = 41 μM, and use-dependent block (black) with IC_{50} = 10.4 μM. (C) Use-dependent block following a train of depolarizations applied at 1 Hz (20 pulses) with IC_{50} = 10.4 μM (black). Blue and red curves represent use-dependent block by T206S and T206A mutants with IC_{50} = 40 and 60 μM, respectively. (D) Current records for control and resting-state block by 50 or 100 μM diltiazem during a single depolarization, and use-dependent block by 10 or 100 μM diltiazem during trains of depolarizations.

These observations suggest that diltiazem has a higher affinity for the channel in the open and inactivated states, consistent with the modulated receptor hypothesis (Hille, 1977), which postulates that the state of the channel influences drug binding to a site located within the pore in a voltage- and state-dependent manner (Hille, 1977; Lee and Tsien, 1983; Hondeghem and Katzung, 1984). Remarkably, the IC_{50} value for diltiazem in blocking Ca_VAb matches its potency against the mammalian cardiac Ca^{2+} channel $Ca_V1.2$ almost exactly, further validating the relevance of Ca_VAb as a model for studying the structural basis for drug block.

Diltiazem Binding to the Intracellular Side of the Ion Selectivity Filter. In mammalian $Ca_V1.2$ channels, photoaffinity labeling and site-directed mutagenesis studies suggest that diltiazem binds to a receptor site formed by the pore-lining transmembrane segments IIIS6 and IVS6 (Hering et al., 1996; Kraus et al., 1996, 1998; Hockerman et al., 1997, 2000). To map the diltiazem-binding site in three dimensions, we crystallized and determined the structure of the diltiazem-Ca_VAb complex at 3.2 Å resolution. As expected, the diltiazem-Ca_VAb complex adopts a nearly 4-fold symmetric structure (Fig. 2, A and B). Diltiazem binds to the intracellular side of the selectivity filter and the nearby walls of the central cavity (Fig. 2, B and C) by displacing lipids present in the apo-Ca_VAb structure (Payandeh et al., 2011, 2012). The bound drug precisely fits the extra electron density observed in the drug-bound Ca_VAb complex (Fig. 2C).

As initially revealed for Na_VAb (Payandeh et al., 2011), fenestrations penetrate the sides of the central cavities in both Na_V and Ca_V channels and connect them to the surrounding lipid bilayer membrane in situ or to the bicelle lipid phase in our crystals (Wu et al., 2016; Pan et al., 2018). When bound to Ca_VAb, the methoxybenzene ring of diltiazem points toward the fenestration formed between two adjacent S6 helices, making hydrophobic contacts with M209 on S6 of one subunit and T206 on S6 of the neighboring subunit (Fig. 2C; see also Fig. 4B). By bridging two subunits, this binding pose may induce allosteric interactions. M174 and T175 from the P-loop of the neighboring subunit are also in close proximity to the methoxy-aromatic ring and contribute to its binding and to allosteric interactions between subunits (Fig. 2C). The central 1,5-benzothiazepine scaffold of diltiazem lies horizontally beneath the P-helix of one subunit in parallel to the lipid bilayer, with its sulfur atom positioned near the central axis of the pore (Fig. 2, B and C). The tertiary amino group of bound diltiazem is positioned on the intracellular side of the bound drug molecule, facing the central cavity, and the acetyl branch of diltiazem is oriented toward the innermost Ca^{2+}-binding site in the selectivity filter (Site 3), which is unoccupied. T175 and L176 of one P-loop and L176 of an adjacent P-loop appear to hold the 1,5-benzothiazepine moiety in place via hydrophobic interactions from the top (Fig. 2, B and C). Thus, diltiazem occupies the top half of the central cavity of Ca_VAb and effectively blocks the exit of Ca^{2+} from the intracellular side of the narrow selectivity filter.

Comparison of the structures of Ca_VAb in complex with diltiazem and Br-verapamil reveals that the diltiazem-binding site partially overlaps with that of the PAA (Fig. 3), consistent with competitive binding interactions observed in ligand-binding studies (Kraus et al., 1998). Interestingly, the monomethoxybenzene group of diltiazem and the dimethoxybenzene group of Br-verapamil share a similar binding pose in the Ca_VAb central cavity and both directly contact T206, a key residue in channel inactivation (Gamal El-Din et al., 2019). Mutation of T206 not only impairs Br-verapamil block of Ca_VAb, but also increases the IC_{50} value of diltiazem for use-dependent inhibition of the channel (Fig. 1C). Mutation to Ser increases the IC_{50} value of diltiazem by 4-fold, and mutation to Ala further increases the IC_{50} value by 6-fold (Fig. 1C), indicating an important role of this residue in determining state-dependent block by both of these classes of drugs (Lee and Tsien, 1983).

Allosteric Interaction between Diltiazem and DHPs on Ca_VAb. Previous mutagenesis studies indicated partial overlap of IIIS6 and IVS6 residues that are important for DHP binding with those that are important for diltiazem binding (Kraus et al., 1996, 1998; Hockerman et al., 2000; Dilmac et al., 2003). Diltiazem inhibits PAA binding but stimulates DHP binding to $Ca_V1.2$ channels by allosteric mechanisms

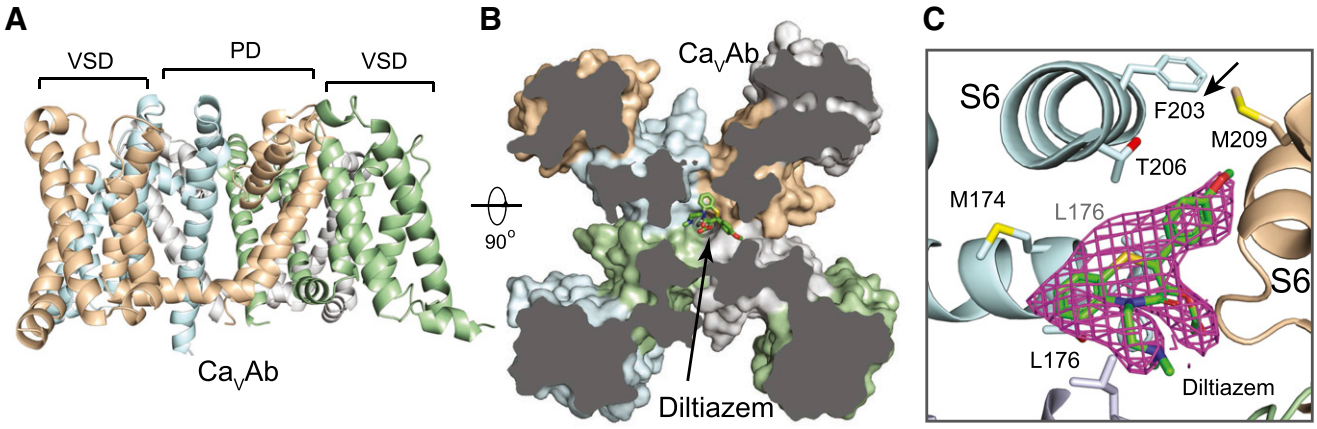

Fig. 2. Structural basis of Ca_vAb block by diltiazem. (A) Overall structure of Ca_vAb illustrated with each subunit distinctly colored (PD, pore domain; VSD, voltage-sensing domain). (B) A cross-sectional view of Ca_vAb in complex with diltiazem. (C) A close-up view of diltiazem binding at the intracellular side of the selectivity filter. Diltiazem is shown in stick model fitting into an F_o-F_c omit map colored in magenta and contoured at 3σ. Nearby side chains are highlighted and shown as sticks. An arrow is shown to mark the position of the fenestration in Ca_vAb (S6, S6-helix; P, P-helix).

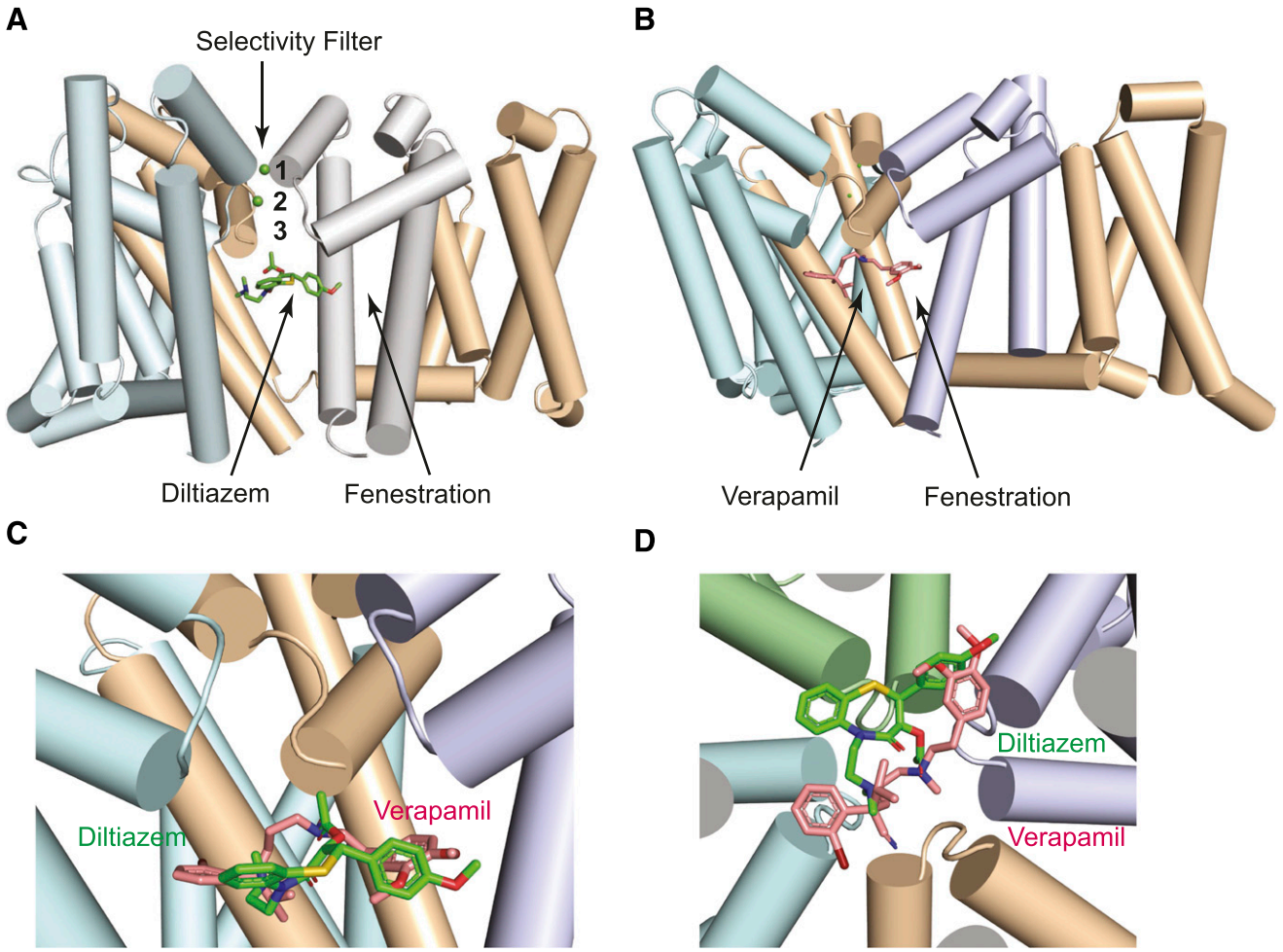

Fig. 3. Comparison of Ca_vAb block by diltiazem and verapamil. (A) Side view of Ca_VAb with diltiazem (sticks in green) bound underneath the selectivity filter. Ca^{2+} is shown as green spheres. The three calcium-binding sites are indicated by the numbers 1, 2, and 3. Portions of the channel are omitted for clarity. (B) Side view of Ca_VAb with Br-verapamil (sticks in pink) bound reveals overlap between the binding sites of the PAA drug and diltiazem. (C) Side view of Ca_vAb as in (A and B), with superposition of bound diltiazem (green sticks) and verapamil (pink sticks). (D) Orthogonal view of the central cavity of Ca_vAb, showing the overlapping PAA/BZT-binding sites as if one were standing at the bottom of the central cavity and looking upward at the selectivity filter.

(Murphy et al., 1983; Goll et al., 1984; Striessnig et al., 1986). Therefore, BZTs and DHPs most likely target Ca^{2+} channels at distinct, but possibly overlapping, binding sites. By comparison with our previous structure of Ca_VAb in complex with the DHP amlodipine, the diltiazem-binding site is indeed physically separate from the DHP-binding site, which is located at an intersubunit crevice on the lipid-facing surface of the pore module. To investigate the structural basis for the allosteric interactions between these sites, we determined the crystal structure of Ca_VAb with both diltiazem and amlodipine bound. Consistent with the structural results obtained with the two antagonists individually, diltiazem and amlodipine are engaged with their respective binding sites on two sides of the S6 segments that form the wall of the Ca_VAb pore module (Fig. 4, A and B). Bound diltiazem is located inside the pore, whereas amlodipine is more than 11 Å away, docking at the outer lipid-facing surface of the pore, which is separated from the diltiazem site by the S6 segments.

The structure of the diltiazem-Ca_VAb in complex with amlodipine reveals changes in the binding pose of diltiazem (Fig. 4, C and D). The distinct binding poses of diltiazem in the absence and presence of amlodipine are illustrated at higher resolution with the associated electron density maps in Supplemental Fig. 1. Similar to its binding mode without the DHPs, the central 1,5-benzothiazepine scaffold of diltiazem lies parallel to the lipid bilayer underneath the selectivity filter. However, compared with the Ca_VAb complex with diltiazem alone, the 1,5-benzothiazepine scaffold is flipped by ~180° and the methoxylbenezene moiety is inserted deeper into the fenestration (Fig. 4, C and D; Supplemental Fig. 1). As a result, the positively charged tertiary amino group extends toward the intracellular end of the narrow passage through the selectivity filter and approaches the backbone carbonyl group of Thr175. This backbone carbonyl contributes to the inner Ca^{2+} coordination site (Site 3) in the selectivity filter, which has the lowest affinity of the three Ca^{2+}-binding sites and is unoccupied by Ca^{2+} in the presence of diltiazem in our crystals.

Comparison between the diltiazem-Ca_VAb-amlodipine and Ca_VAb-amlodipine structures shows that the C-terminal regions of two Ca_VAb subunits become partially ordered when diltiazem is present, suggesting a global conformational change (Fig. 5). We speculate that the structure of diltiazem

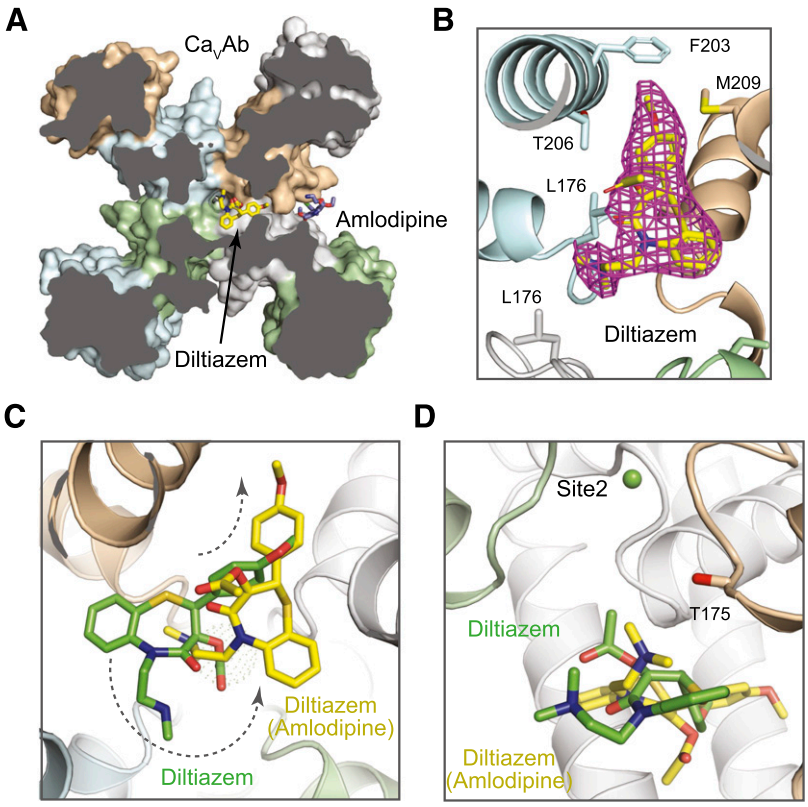

Fig. 4. Structural basis for allosteric interactions between diltiazem and dihydropyridines bound to Ca_vAb. (A) Surface representation of Ca_VAb in complex with diltiazem and amlodipine. (B) Zoom-in view of diltiazem binding at the intracellular side of the selectivity filter. Diltiazem is shown in stick format, along with an F_o-F_c omit map contoured at 3σ. Nearby side chains are highlighted and shown in stick format. (C) Comparison of diltiazem binding to Ca_VAb alone (green) or in the presence of amlodipine (yellow). Dashed arrows indicate the differences between diltiazem positions. (D) Orthogonal view of (C) with calcium bound to the selectivity filter shown in green spheres.

bound with amlodipine represents a higher affinity binding pose with the tertiary amino group inserted into the inner end of the ion selectivity filter to engage Ca^{2+}-binding Site 3 formed by the backbone carbonyls of Thr175 (Figs. 4 and 5). This change in binding pose is induced by conformational changes caused by amlodipine binding, which may be similar to the structural changes in the inactivated state to which both amlodipine and diltiazem bind preferentially. The pose of diltiazem bound alone might represent an intermediate state of diltiazem binding, in which the drug has not yet taken its final high-affinity position to plug the selectivity filter. Thus, our structures reveal plasticity of diltiazem binding induced by allosteric interactions with DHP binding and potentially by the conformational transition to the inactivated state.

Diltiazem and DHPs Alter Ca^{2+} Binding. Besides physically blocking the ion-conduction pathway, diltiazem also alters the interactions between Ca^{2+} and the selectivity filter of Ca_VAb (Fig. 6). In the diltiazem-Ca_VAb structure, we observed electron densities at both Sites 1 and 2, which most likely represent bound Ca^{2+} (Tang et al., 2014). Strikingly, unlike Ca^{2+} bound to the unblocked channel, these bound ions are off the central axis of the pore when diltiazem is bound (Fig. 6, A and C; see also the electron density map in Supplemental Fig. 1). Ca^{2+} in Site 1 interacts directly with the carboxyl group of one of four D178 residues, suggesting that it is in a partially dehydrated state. This blocker-induced direct interaction between the Ca^{2+} at Site 1 and the selectivity filter is very similar to the proposed mechanism by which DHPs allosterically block Ca_VAb (Tang et al., 2014). These changes in Ca^{2+} binding provide a plausible explanation for potentiation of diltiazem binding by Ca^{2+} (Dilmac et al., 2003) and for the allosteric interactions between amlodipine and diltiazem. Consistent with the notion that the diltiazem-Ca_VAb-amlodipine structure has captured diltiazem transitioning into its high-affinity bound form, Ca^{2+} bound at Site 1 interacts with a D178 carboxyl side chain that has rotated around one torsion angle to form a hydrogen-bonding network with neighboring side chains (Fig. 6B). This side chain rotation resembles the dunking motion of E177 side chains of Na_VAb as they interact with entering Na^+ ions (Chakrabarti et al., 2013); therefore, it is likely to represent a normal conformational transition of the pore.

Discussion

Diltiazem Binds in the Central Cavity and Physically Blocks Ca^{2+} Permeation. Our structural analysis of diltiazem block of Ca_VAb has mapped its binding site on the Ca^{2+} channel in three dimensions in detail. The BZT receptor site is located in the central cavity of the pore, just on the intracellular side of the ion selectivity filter. In this position, diltiazem would prevent conductance of Ca^{2+} by physically blocking it. This binding position is consistent with electrophysiological results, which show that diltiazem completely blocks Ca^{2+} current.

Diltiazem Binding Overlaps the PAA Receptor Site. Radioligand-binding studies have suggested a complex allosteric/competitive binding interaction between BZTs and PAAs. Binding of PAAs was inhibited by diltiazem but substantial PAA binding remained at apparently saturating concentrations of PAAs, consistent with an indirect negative allosteric interaction (Goll et al., 1984). On the other hand,

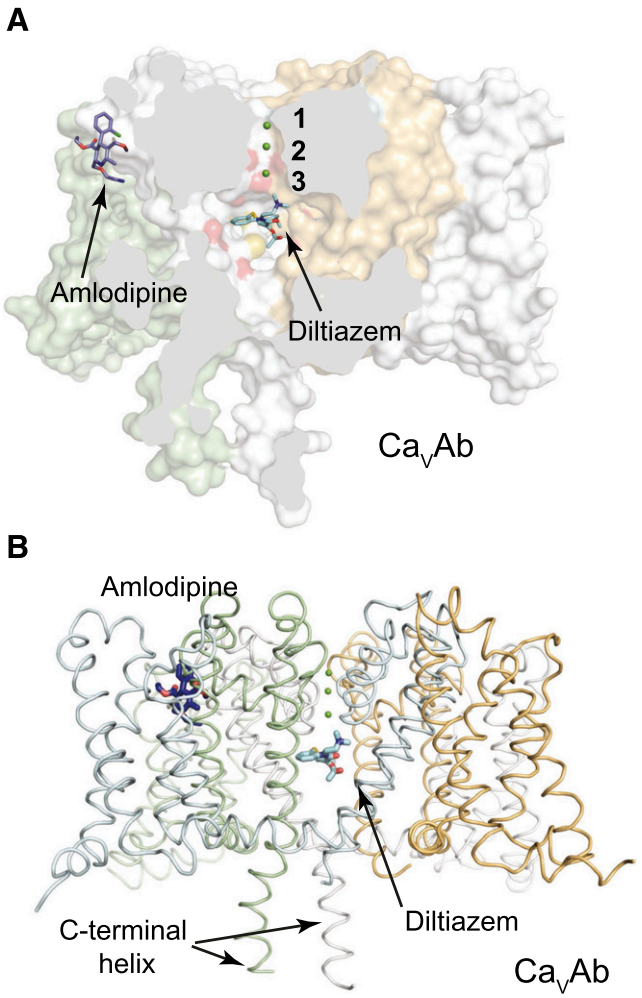

Fig. 5. Structural basis for inhibition of Ca_VAb by amlodipine and diltiazem in combination. (A) Surface representation of diltiazem and amlodipine bound to Ca_VAb reveals that these drugs bind to different sides of S6. (B) Overall structure of diltiazem-CavAb-amlodipine shown as ribbons.

extensive molecular mapping studies using photoaffinity labeling and site-directed mutagenesis revealed overlapping amino acid residues in the BZT and PAA receptor sites (Kraus et al., 1996; Dilmac et al., 2003). Our results are consistent with both aspects of this previous work. On one hand, we show that the diltiazem-binding site clearly overlaps with the PAA-binding site. On the other hand, our results reveal complexities of diltiazem binding that may lead to allosteric/competitive interactions. We find that diltiazem has two binding poses that can be allosterically modulated by amlodipine binding and potentially by voltage-dependent inactivation. The lower affinity binding pose of diltiazem may leave room for PAA binding in their overlapping sites, thereby inducing a mixed allosteric/competitive mode of inhibition in ligand-binding studies.

Diltiazem Interacts Allosterically with Amlodipine. We previously found that binding of amlodipine induces a global conformational change in Ca_VAb, which alters its quaternary structure (Tang et al., 2016). Our present studies reveal the structural basis for allosteric interaction between diltiazem and dihydropyridines, consistent with the allosteric binding interactions observed in classic ligand-binding studies of Ca_V channels (Murphy et al., 1983; Striessnig et al., 1986). Amlodipine binding also modifies the coordination of Ca^{2+}, bringing one Ca^{2+} ion close to the carboxylate side chain of the D178 residue in the Ca_VAb subunit that binds amlodipine (Tang et al., 2016). In this study, we also found that drug binding alters the coordination of Ca^{2+}; that is, diltiazem binding to its site in the central cavity induces an allosteric change in Ca^{2+} coordination. As for amlodipine, it is likely that this change in Ca^{2+} coordination greatly reduces or blocks ion conductance through the pore.

Diltiazem Binding May Be a Two-Step Process. Our structures reveal diltiazem in two binding poses. In the absence of other drugs, diltiazem binds loosely to the upper walls of the central cavity, in what appears to be a low-affinity binding mode, but it does not penetrate the ion selectivity filter. In the presence of amlodipine, diltiazem binding appears tighter, and its tertiary amino group extends upward into the inner end of the selectivity filter and interacts with Site 3 formed by the backbone carbonyls of T175. We speculate that this binding pose may be favored by voltage-dependent inactivation, which is also favored by amlodipine binding. Detailed studies of the kinetics of diltiazem binding have also suggested the possibility of two distinct binding poses and partial stepwise binding interactions (Prinz and Striessnig, 1993). Thus, in the absence of other drugs, diltiazem may enter the pore, form a loose channel-blocking complex, and then rearrange to a tighter-binding, more stably blocked complex with bound diltiazem projecting into the selectivity filter from the central cavity upon voltage-dependent inactivation. Conformational changes in the ion selectivity filter that we observed upon inactivation of Na_VAb may be responsible for this change in binding of diltiazem.

Diltiazem Binding Modulates Ca^{2+} Binding in the Selectivity Filter. Allosteric interactions of bound diltiazem induce high-affinity binding of Ca^{2+} in the pore, as judged by close the interaction of bound Ca^{2+} with one D178 side chain. This allosteric change in Ca^{2+} binding may contribute to pore block and to the energetics of allosteric interactions between the two drug-binding sites. Thus, our structures unveil, at the atomic level, the mechanism of pore block and allosteric interactions of this important class of Ca^{2+}-channel blockers and provide guidance and strategy for developing next-generation BZTs with improved potency and specificity.

Comparison with Ca^{2+} Antagonist Receptor Sites on Mammalian Ca_V Channels. As we prepared this paper for submission, a cryoelectron microscopy study of skeletal muscle $Ca_V1.1$ channels revealed the structures of the receptor sites for PAAs, DHPs, and BZTs at high resolution in that channel type (Zhao et al., 2019). Although the $Ca_V1.1$ channels are not themselves a pharmacological target for Ca^{2+} antagonists, they are modulated by these drugs in a similar manner as the cardiac/vascular smooth muscle $Ca_V1.2$ channels that are the in vivo drug targets; however, $Ca_V1.1$ channels typically have lower affinity for Ca^{2+} antagonist drug binding. As we show here, diltiazem bound to a site in the central cavity of $Ca_V1.1$, just on the intracellular side of the ion selectivity filter overlapping the PAA-binding site. The binding pose of diltiazem in $Ca_V1.1$ is most similar to the pose we observe in the presence of amlodipine, which is potentially a higher affinity binding configuration stimulated by

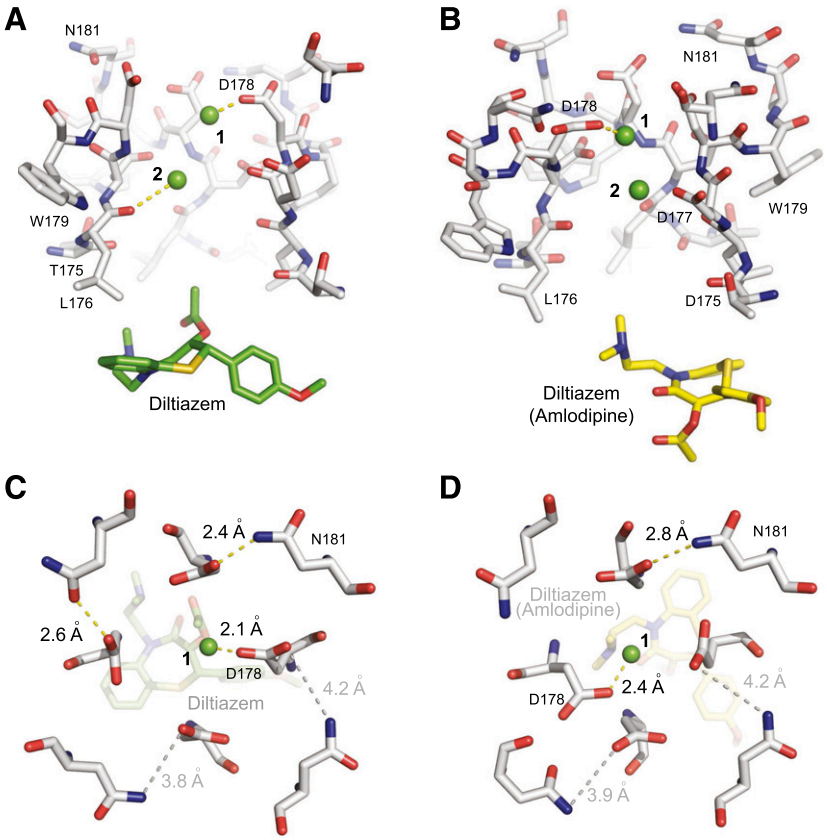

Fig. 6. Diltiazem binding modifies Ca^{2+} binding in the selectivity filter of Ca_vAb. (A and B) Comparisons of selectivity filter ions in the presence of diltiazem (left) and diltiazem + amlodipine (right). Selectivity filter residues 175–179 and diltiazem are shown in stick format, with Ca^{2+} shown as green spheres and hydrogen bonds shown as dashed yellow lines. (C and D) Comparisons of Ca^{2+} bound in Site 1 between diltiazem (left) and diltiazem + amlodipine (right). Side chains from D178 and N181 are shown in each case, along with Ca^{2+} (green spheres), hydrogen bonds (dashed yellow lines), and estimated intermolecular distances (dashed gray lines).

transition to an inactivated state. Overall, there is remarkable agreement between the BZT binding to bacterial and mammalian Ca_V channels, suggesting that the details of allosteric modulation of amlodipine and Ca^{2+} binding that we have observed here in Ca_VAb may also be relevant for mammalian Ca_V channels.

Acknowledgments

We are grateful to the beamline staff at the Advanced Light Source (BL8.2.1 and BL8.2.2) for assistance during data collection and to Dr. Jin Li for technical and editorial support.

Authorship Contributions

Participated in research design: Tang, Gamal El-Din, Zheng, Catterall.

Conducted experiments: Tang, Gamal El-Din.

Performed data analysis: Tang, Gamal El-Din, Lenaeus.

Wrote or contributed to the writing of the manuscript: Tang, Zheng, Gamal El-Din, Lenaeus, Catterall.

References

Catterall WA (2000) Structure and regulation of voltage-gated Ca^{2+} channels. *Annu Rev Cell Dev Biol* **16**:521–555.

Catterall WA (2011) Voltage-gated calcium channels. *Cold Spring Harb Perspect Biol* **3**:a003947.

Chakrabarti N, Ing C, Payandeh J, Zheng N, Catterall WA, and Pomès R (2013) Catalysis of Na^+ permeation in the bacterial sodium channel Na_VAb. *Proc Natl Acad Sci USA* **110**:11331–11336.

Dilmac N, Hilliard N, and Hockerman GH (2003) Molecular determinants of Ca^{2+} potentiation of diltiazem block and Ca^{2+}-dependent inactivation in the pore region of $Ca_v1.2$. *Mol Pharmacol* **64**:491–501.

Gamal El-Din TM, Lenaeus MJ, Ramanadane K, Zheng N, and Catterall WA (2019) Molecular dissection of multiphase inactivation of the bacterial sodium channel Na_VAb. *J Gen Physiol* **151**:174–185.

Godfraind T (2017) Discovery and development of calcium channel blockers. *Front Pharmacol* **8**:286.

Goll A, Ferry DR, Striessnig J, Schober M, and Glossmann H (1984) (−)-[^{3}H] Desmethoxyverapamil, a novel Ca^{2+} channel probe. Binding characteristics and target size analysis of its receptor in skeletal muscle. *FEBS Lett* **176**: 371–377.

Hering S, Aczél S, Grabner M, Döring F, Berjukow S, Mitterdorfer J, Sinnegger MJ, Striessnig J, Degtiar VE, Wang Z, et al. (1996) Transfer of high sensitivity for benzothiazepines from L-type to class A (BI) calcium channels. *J Biol Chem* **271**:24471–24475.

Hille B (1977) Local anesthetics: hydrophilic and hydrophobic pathways for the drug-receptor reaction. *J Gen Physiol* **69**:497–515.

Hockerman GH, Dilmac N, Scheuer T, and Catterall WA (2000) Molecular determinants of diltiazem block in domains IIIS6 and IVS6 of L-type Ca^{2+} channels. *Mol Pharmacol* **58**:1264–1270.

Hockerman GH, Peterson BZ, Johnson BD, and Catterall WA (1997) Molecular determinants of drug binding and action on L-type calcium channels. *Annu Rev Pharmacol Toxicol* **37**:361–396.

Hondeghem LM and Katzung BG (1984) Antiarrhythmic agents: the modulated receptor mechanism of action of sodium and calcium channel-blocking drugs. *Annu Rev Pharmacol Toxicol* **24**:387–423.

Kraus R, Reichl B, Kimball SD, Grabner M, Murphy BJ, Catterall WA, and Striessnig J (1996) Identification of benz(othi)azepine-binding regions within L-type calcium channel $\alpha 1$ subunits. *J Biol Chem* **271**:20113–20118.

Kraus RL, Hering S, Grabner M, Ostler D, and Striessnig J (1998) Molecular mechanism of diltiazem interaction with L-type Ca^{2+} channels. *J Biol Chem* **273**: 27205–27212.

Lee KS and Tsien RW (1983) Mechanism of calcium channel blockade by verapamil, D600, diltiazem and nitrendipine in single dialysed heart cells. *Nature* **302**: 790–794.

Murphy KMM, Gould RJ, Largent BL, and Snyder SH (1983) A unitary mechanism of calcium antagonist drug action. *Proc Natl Acad Sci USA* **80**:860–864.

Pan X, Li Z, Zhou Q, Shen H, Wu K, Huang X, Chen J, Zhang J, Zhu X, Lei J, et al. (2018) Structure of the human voltage-gated sodium channel $Na_v1.4$ in complex with $\beta 1$. *Science* **362**:eaau2486.

Payandeh J, Gamal El-Din TM, Scheuer T, Zheng N, and Catterall WA (2012) Crystal structure of a voltage-gated sodium channel in two potentially inactivated states. *Nature* **486**:135–139.

Payandeh J, Scheuer T, Zheng N, and Catterall WA (2011) The crystal structure of a voltage-gated sodium channel. *Nature* **475**:353–358.

Prinz H and Striessnig J (1993) Ligand-induced accelerated dissociation of (+)-*cis*-diltiazem from L-type Ca^{2+} channels is simply explained by competition for individual attachment points. *J Biol Chem* **268**:18580–18585.

Ren D, Navarro B, Xu H, Yue L, Shi Q, and Clapham DE (2001) A prokaryotic voltage-gated sodium channel. *Science* **294**:2372–2375.

Striessnig J, Goll A, Moosburger K, and Glossmann H (1986) Purified calcium channels have three allosterically coupled drug receptors. *FEBS Lett* **197**: 204–210.

Tamariz LJ and Bass EB (2004) Pharmacological rate control of atrial fibrillation. *Cardiol Clin* **22**:35–45.

Tang L, Gamal El-Din TM, Payandeh J, Martinez GQ, Heard TM, Scheuer T, Zheng N, and Catterall WA (2014) Structural basis for Ca^{2+} selectivity of a voltage-gated calcium channel. *Nature* **505**:56–61.

Tang L, Gamal El-Din TM, Swanson TM, Pryde DC, Scheuer T, Zheng N, and Catterall WA (2016) Structural basis for inhibition of a voltage-gated Ca^{2+} channel by Ca^{2+} antagonist drugs. *Nature* **537**:117–121.

Triggle DJ (2007) Calcium channel antagonists: clinical uses—past, present and future. *Biochem Pharmacol* **74**:1–9.

Wu J, Yan Z, Li Z, Qian X, Lu S, Dong M, Zhou Q, and Yan N (2016) Structure of the voltage-gated calcium channel $Ca_v1.1$ at 3.6 Å resolution. *Nature* **537**: 191–196.

Zamponi GW, Striessnig J, Koschak A, and Dolphin AC (2015) The physiology, pathology, and pharmacology of voltage-gated calcium channels and their future therapeutic potential. *Pharmacol Rev* **67**:821–870.

Zhao Y, Huang G, Wu J, Wu Q, Gao S, Yan Z, Lei J, and Yan N (2019) Molecular basis for ligand modulation of a mammalian voltage-gated Ca^{2+} channel. *Cell* **177**: 1495–1506.e12.

Address correspondence to: Lin Tang, Department of Neurology, State Key Laboratory of Biotherapy and Cancer Center, West China Hospital, Sichuan University and Collaborative Innovation Center for Biotherapy, Chengdu, Sichuan, China. E-mail: ltang@scu.edu.cn; or Ning Zheng, Department of Pharmacology, Howard Hughes Medical Institute, University of Washington, Seattle, WA 98195-7280. E-mail: nzheng@uw.edu; or William A. Catterall, Department of Pharmacology, University of Washington, Seattle, WA 98195-7280. E-mail: wcatt@uw.edu

Molecular Pharmacology

Supplementary Information for

Structural Basis for Diltiazem Block of a Voltage-gated Ca^{2+} Channel

Lin Tang[1,2,3‡], Tamer M. Gamal El-Din[2], Michael J. Lenaeus[2, 3], Ning Zheng[2,4‡], and William A. Catterall[2‡]

[1]Department of Neurology, State Key Lab of Biotherapy and Cancer Center, West China Hospital, Sichuan University and Collaborative Innovation Center for Biotherapy, Chengdu, Sichuan, 610041 China; [2]Department of Pharmacology, [3]Division of General Internal Medicine, Department of Medicine, and [4]Howard Hughes Medical Institute, University of Washington, Seattle, WA 98195-7280 USA

‡ Co-corresponding authors
Ning Zheng, Department of Pharmacology, Howard Hughes Medical Institute, University of Washington, Seattle WA 98195-7280, nzheng@uw.edu
William A. Catterall, Department of Pharmacology, University of Washington, Seattle WA 98195-7280, W.A.C., wcatt@uw.edu

This PDF file includes:

Supplementary text
Figures S1
Tables S1

Supplemental Information

Supplemental Methods

Ca_VAb Constructs. As originally defined, Ca_VAb was constructed by introducing the mutations E177D/S178D/M181D into Na_VAb. This construct was used for all electrophysiological studies, except as noted in Figure Legends. In this work, we have also used Ca_VAb E177D/S178D/M181N, which has identical structure and Ca^{2+} binding properties and has high Ca^{2+} selectivity. It gives greater consistency of high-resolution crystal structures. We have also added the mutation W195Y, which substitutes the Y residue from the analogous position in mammalian $Ca_V1.2$ channels for W195 in Ca_VAb. This mutant

gives better resolution of drugs bound at the DHP site. Ca_VAb/E177D/S178D/M181N/W195Y was used for all structural studies presented here, except as noted in the Figure Legends. Similar structural results were obtained for both versions of Ca_VAb.

Electrophysiology. All measurements were done in *T. ni* insect cells (High5) using methods described previously (Gamal El-Din et al., 2018; Gamal El-Din et al., 2013). All Ca_VAb constructs used were made on the background of N49K mutation. Mutation N49K shifts the activation curve ~75 mV to more positive potentials compared to wild type Ca_vAb and abolishes the use-dependent inactivation as previously described previously(Gamal El-Din et al., 2018; Gamal El-Din et al., 2013). All constructs showed good expression, allowing measurement of ionic currents 24–48 h after infection. Whole-cell currents were recorded using an Axopatch 200 amplifier (Molecular Devices) with glass micropipettes (2–4 MΩ). Capacitance was subtracted and 80–90% of series resistance was compensated using internal amplifier circuitry. Extracellular solutions contained in (mM) 10 $BaCl_2$, 140 NMDG-methanesulphonate, 20 HEPES, (pH 7.4, adjusted with $Ba(OH)_2$, $[Ba^{2+}]_{total}$ = 13 mM). Intracellular solutions contained in (mM) 105 CsF, 35 NaCl, 10 HEPES, 10 EGTA, (pH 7.4, adjusted with $CsOH_)$. Current–voltage (*I–V*) relationships were recorded in response to steps to voltages ranging from −120 to +50 mV in 10-mV increments from a holding potential of −120 mV. Conductance-voltage (G-V) curves were calculated from the corresponding (I-V) curves. Pulses were generated and currents were recorded using Pulse software controlling an Instrutech ITC18 interface (HEKA). Data were analysed using Igor Pro 6.2 (WaveMetrics). Sample sizes were chosen to give s.e.m. values of less than 10% of peak values based on prior experimental experience.

Protein Expression and Purification. The pFastBac-FLAG-Ca_VAb was used as the construct for producing homotetrameric model voltage-gated Ca^{2+} channel. I199S, W195Y, T206S and T206A constructs were generated via site-directed mutagenesis using QuickChange (Stratagene). Recombinant baculovirus were produced using the Bac-to-Bac system (Invitrogen), and *T. ni* insect cells were infected for large-scale protein purification. Cells were harvest 72 h post-infection and re-suspended

in buffer A (50 mM Tris-HCl pH=8.0, 200 mM NaCl) supplemented with protease inhibitors and DNase. After sonication, digitonin (EMD Biosciences) was added to 1% and solubilization was carried out for 1-2 h at 4^{o}C. Clarified supernatant was then incubated with anti-Flag M2-agarose resin (Sigma) for 1-2 h at 4 °C with gentle mixing. Flag-resin was washed with ten column volumes of buffer B (buffer A supplemented with 0.12 % digitonin) and eluted with buffer B supplemented with 0.1 mg/ml Flag peptide. The eluent was concentrated and then passed over a Superdex 200 column (GE Healthcare) in 10 mM Tris-HCl pH=8.0, 100 mM NaCl and 0.12 % digitonin. The peak fractions were concentrated using a Vivaspin 30K centrifugal device.

Crystallization and Data Collection. Ca_VAb and its W195Y mutant were concentrated to ~20 mg ml^{-1} and reconstituted into DMPC:CHAPSO (Anatrace) bicelles according to standard protocols. The protein-bicelle preparation and a well solution containing 1.8-2.0 M ammonium sulfate, 100 mM Na-citrate pH=5.0 was mixed with a 1:1 ratio and set up in a hanging-drop vapour-diffusion format. All the antagonist complex crystals were obtained through co-crystallization by incubating the protein-bicelle with 100uM antagonist overnight before setting up crystallization trails. For the diltiazem-amlodipine complex, 100 μM of diltiazem was kept in the purification solutions from the beginning. Crystals are cryoprotected by soaking in 0.1 M Na-citrate pH=5.0, 26% glucose 2.0 M ammonium sulfate, and 2 mM Ca^{2+}. Crystals were then plunged into liquid nitrogen and maintained at 100^{o}K during all data collection procedures.

The anomalous diffraction datasets were collected at 1.0 Å with the same synchrotron radiation source (Advanced Light Source, BL8.2.1).

Structure Determination, Refinement, and Analyses. X-ray diffraction data were integrated and scaled with the HKL2000 package and further processed with the CCP4 package. The structure of Ca_VAb and its antagonist complexes were solved by molecular replacement by using an individual subunit of the Ca_VAb structure (PDB code 4MS2) as the search template. The datasets were processed

in $P22_12_1$ space group and there are four molecules in one asymmetric unit. Crystallography and NMR System software was used for refinement of coordinates and *B*-factors. Final models were obtained after several cycles of refinement with REFMAC and PHENIX and manual re-building using program COOT. The geometries of the final structural models of Ca_VAb and its antagonist complexes were verified using PROCHEC. Detailed crystallographic data and refinement statics for all the constructs are shown in Table S1. All structural figures were prepared with the PyMol software.

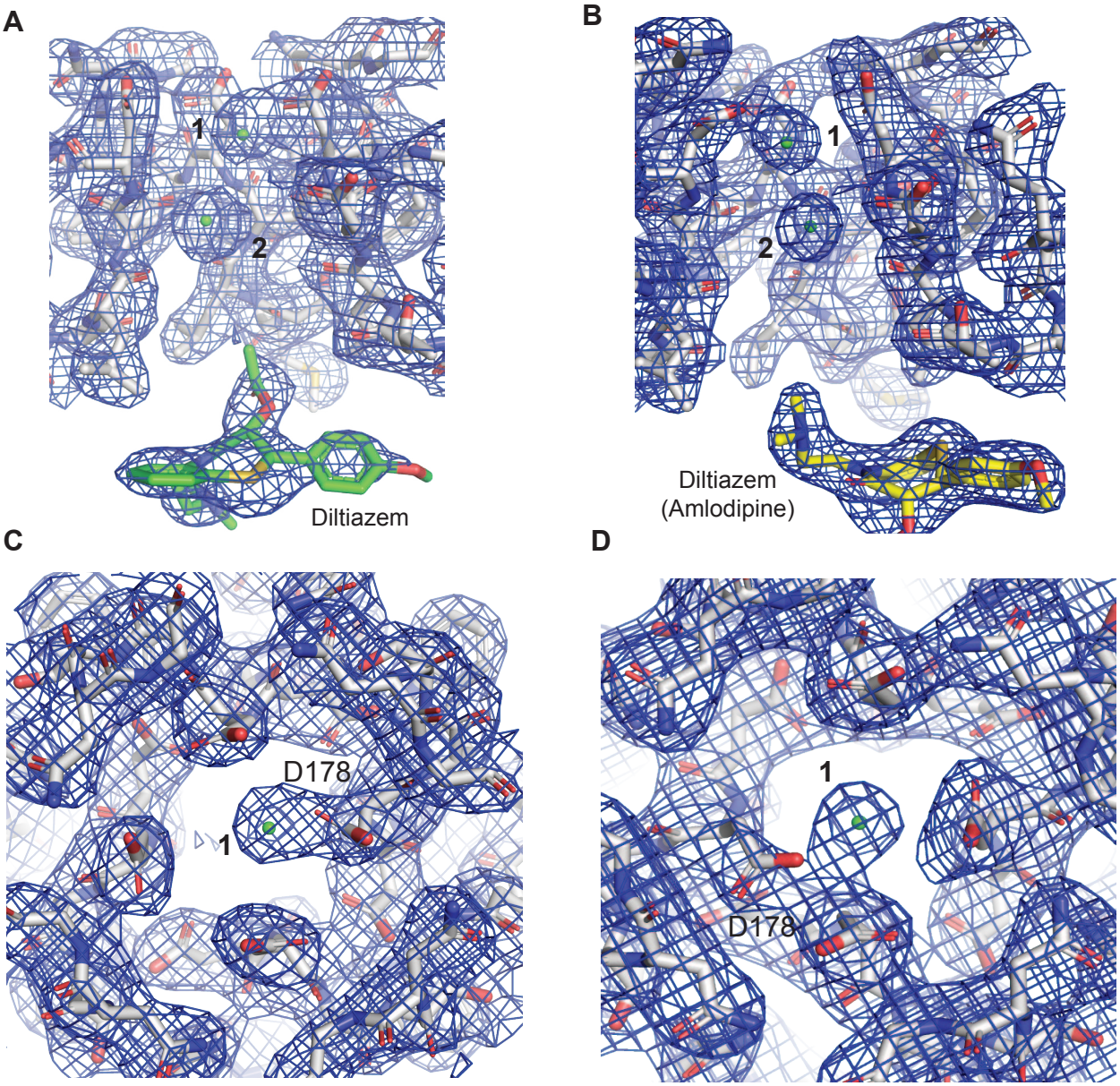

Supplemental Figure 1. Electron density to support allosteric conformational changes in drug binding positions and Ca^{2+} binding sites. A, Side view of the selectivity filter of Ca_VAb in complex with diltiazem, with one subunit removed for clarity. The model is shown in stick format with diltiazem and Ca^{2+} in green. 2Fo-Fc electron density is shown, contoured at 2 σ. B, Model and electron density for Ca_VAb/diltiazem/amlodipine complex, displayed as in panel A. C, 2Fo-Fc electron density (contoured at 2 σ) is shown for Site 1 calcium ion in the Ca_VAb/diltiazem structure. The view is restricted to D178 and N181 for clarity. D, 2fo-fc electron density (contoured at 2 σ) is shown for Ca^{2+} at Site 1 in the Ca_VAb/diltiazem/amlodipine structure. Note that one D178 side chain has changed its rotamer and is now close enough to an adjacent subunit to form a hydrogen bonding network.

Supplemental Table 1.
Data collection, phasing and refinement statistics

	Ca_vAb Diltiazem 5mM Ca^{2+}	Ca_vAb Amlodipine Diltiazem 5mM Ca^{2+}
Data collection		
Space group	P22121	P22121
Cell dimensions		
a, *b*, *c* (Å)	125.6 125.6 191.8	124.7 124.9 191.9
α, β, γ (°)	90 90 90	90 90 90
Resolution (Å)	3.2	3.0
R_{sym} or R_{merge}	13.9(61.1)	8.8(35.2-)
$CC_{1/2}$(%)	99.4 (80.5)	99.4(87.2)
$I/\sigma I$	9.5(2.4)	12.1(3.7)
Completeness (%)	90.5(91.8)	91.1(91.8)
Redundancy	5.2(5.2)	4.9(4.6)
Refinement		
Resolution (Å)	30-3.2	44.8-3.0
No. reflections	45638	54805
R_{work}/ R_{free}	22.8/26.7	23.7/28.6
No. atoms	7471	7849
Protein	7269	7402
Ligand/ion	195	441
Water		
B-factors		
Protein	86.5	80.7
Ligand/ion	86.4	102.3
Water		
R.m.s deviations		
Bond lengths (Å)	0.012	0.015
Bond angles (°)	1.58	1.61